NeuroImage: Clinical 31 (2021) 102739

Contents lists available at ScienceDirect

NeuroImage: Clinical

journal homepage: www.elsevier.com/locate/ynicl

Diffuse white matter abnormality in very preterm infants at term reflects reduced brain network efficiency

Julia E. Kline [a], Venkata Sita Priyanka Illapani [a], Hailong Li [a], Lili He [a,b], Weihong Yuan [c,d], Nehal A. Parikh [a,b,c,*]

[a] Perinatal Institute, Cincinnati Children's Hospital Medical Center, Cincinnati, OH, United States
[b] Department of Pediatrics, University of Cincinnati College of Medicine, Cincinnati, OH, United States
[c] Pediatric Neuroimaging Research Consortium, Cincinnati Children's Hospital Medical Center, Cincinnati, OH, United States
[d] Department of Radiology, University of Cincinnati College of Medicine, Cincinnati, OH, United States

ARTICLE INFO

Keywords:
Very preterm
diffusion MRI
Graph theory
Diffuse white matter abnormality

ABSTRACT

Between 50 and 80% of very preterm infants (<32 weeks gestational age) exhibit increased white matter signal intensity on T2-weighted MRI at term-equivalent age, known as diffuse white matter abnormality (DWMA). A few studies have linked DWMA with microstructural abnormalities, but the exact relationship remains poorly understood. We related DWMA extent to graph theory measures of network efficiency at term in a representative cohort of 343 very preterm infants. We performed anatomic and diffusion MRI at term and quantified DWMA volume with our novel, semi-automated algorithm. From diffusion-weighted structural connectomes, we calculated the graph theory metrics local efficiency and clustering coefficient, which measure the ability of groups of nodes to perform specialized processing, and global efficiency, which assesses the ability of brain regions to efficiently combine information. We computed partial correlations between these measures and DWMA volume, adjusted for confounders. Increasing DWMA volume was associated with decreased global efficiency of the entire very preterm brain and decreased local efficiency and clustering coefficient in a variety of regions supporting cognitive, linguistic, and motor function. We show that DWMA is associated with widespread decreased brain network efficiency, suggesting that it is pathologic and likely has adverse developmental consequences.

1. Introduction

Up to 80% of very preterm infants exhibit increased white matter signal intensity on T2-weighted MRI at term-equivalent age (Skiöld, 2010; Jeon et al., 2012). This hyperintense signal, referred to as either diffuse excessive high signal intensity (DEHSI) or diffuse white matter abnormality (DWMA), has been investigated in relation to neurodevelopmental outcomes in premature infants with mixed results. Some studies have shown no significant relationship between DWMA and later neurodevelopmental deficits, including cognitive, language, and motor impairments (Jeon et al., 2012; Kidokoro et al., 2011; Broström et al., 2016; Hart, 2011; de Bruïne et al., 2011; Skiöld, 2012; Mürner-Lavanchy et al., 2019; Calloni, 2015; Leitner, 2014). Conversely, other studies (Boardman et al., 2010; Krishnan et al., 2007; Iwata et al., 2012; Iwata, 2007), especially those that quantified DWMA extent at term age (Parikh, 2013; Parikh et al., 2020a, 2020b), identified significant associations with neurodevelopmental outcomes, particularly cognition and language.

The cellular pathology and brain connectivity alterations underlying DWMA have not been fully delineated. In pilot studies of preterm infants with DWMA, abnormal white matter microstructure on diffusion MRI (Skiöld, 2010; Counsell, 2006) and aberrant functional connectivity derived from resting state fMRI (He and Parikh, 2015) were documented at term. A small postmortem histopathology case series from our group reported fewer oligodendroglial cells and axons in the brains of very preterm infants in regions of DWMA compared to the brains of control infants (Parikh et al., 2016). Based on these results, we postulated that DWMA is associated with brain network disorganization in very preterm infants.

Graph theory is a powerful mathematical method that can investigate the information transfer and processing capacity of complex networks like the human brain (Bullmore and Sporns, 2009; Rubinov and

* Corresponding author at: Cincinnati Children's Hospital, 3333 Burnet Ave, MLC 7009, Cincinnati, OH 45229, United States.
E-mail address: Nehal.Parikh@cchmc.org (N.A. Parikh).

https://doi.org/10.1016/j.nicl.2021.102739
Received 26 March 2021; Received in revised form 28 May 2021; Accepted 21 June 2021
Available online 25 June 2021

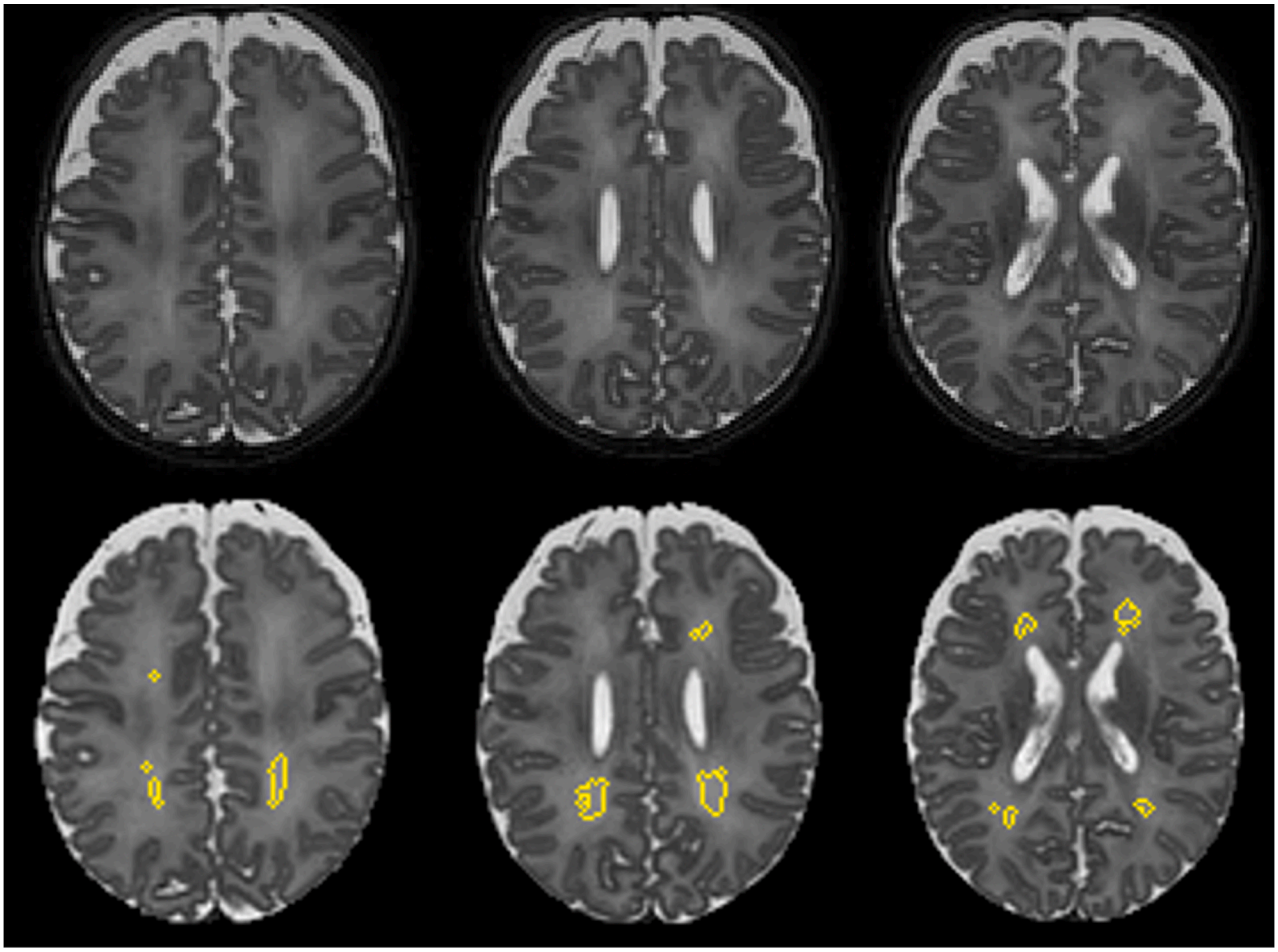

Fig. 1. Example Semi-automated DWMA Segmentation. The top row shows three slices from a T2-weighted MRI scan of the same male infant; gestational age of 25.4 weeks, postmenstrual age at MRI of 41.7 weeks. The bottom row displays the same slices with clusters of voxels designated as DWMA by our algorithm circled in yellow. (For interpretation of the references to colour in this figure legend, the reader is referred to the web version of this article.)

Sporns, 2010; Sporns and Zwi, 2004; Sporns, 2013; Bassett et al., 2017). The brain's connectome can be modeled as a set of regions (nodes) and their pair-wise associations (edge weights), which may represent number of structural connections, effective or functional connectivity values, or measures of white matter integrity between regions. From symmetric matrices of edge weights, graph metrics can be calculated that quantify high-level brain network properties. Although some graph metrics are preserved in prematurity (Ball et al., 2014; Scheinost et al., 2016; Bouyssi-Kobar et al., 2019), a subset including global efficiency (E_{glob}), local efficiency (E_{loc}), and clustering coefficient (CC), are altered by preterm birth (Bouyssi-Kobar et al., 2019; Young, 2018; Gozdas, 2018), and these alterations may be the antecedents of lifelong neurodevelopmental impairment (Thompson et al., 2016).

Our main objective was to quantify DWMA in a regional, population-based cohort of very preterm infants using our published semi-automated algorithm and to quantify the relationship between DWMA volume and graph theory metrics of information processing efficiency: E_{glob}, E_{loc}, and CC, correcting for known confounders of early brain development in very preterm infants. We hypothesized that global efficiency would decrease with increasing extent of objectively-quantified DWMA. Likewise, we hypothesized that E_{loc} and CC would decrease with increasing DWMA volume, particularly in regions related to cognition, language, and motor ability.

2. Materials and methods

2.1. Subjects

We enrolled a multicenter, prospective cohort of 343 very preterm infants (gestational age [GA] $\leq$ 32 weeks) from five level-III Greater Cincinnati area neonatal intensive care units: 1) Cincinnati Children's Hospital Medical Center, Cincinnati's primary academic pediatric referral service for the sickest neonates; 2) University of Cincinnati Medical Center, Cincinnati's primary academic hospital for high-risk maternal referral; 3) Good Samaritan Hospital; 4) Kettering Medical Center;

and 5) St. Elizabeth's Healthcare; the latter three represent non-academic sites. Subjects were recruited between June 2017 and November 2019 and were excluded if they had cyanotic heart disease or chromosomal or congenital anomalies affecting their central nervous system. Infants who were hospitalized and mechanically ventilated on more than 50% supplemental oxygen at 45-weeks postmenstrual age (PMA) were also excluded. All experimental protocols involving human subjects were in accordance with the Declaration of Helsinki. The Cincinnati Children's Hospital Institutional Review Board approved this study, resulting in approval at the other sites due to reciprocity agreements. A parent or guardian of each infant gave written informed consent before enrollment.

2.2. MRI data acquisition

All study infants were imaged during unsedated sleep between 40- and 44- weeks postmenstrual age on a 3 T Philips Ingenia scanner (Philips Medical Systems, Best, the Netherlands) with a 32 channel phase array head coil. All MRI scans were performed at Cincinnati Children's Hospital using identical imaging parameters. A skilled neonatal nurse and neonatologist were both present for any scan requiring positive pressure airway support. Each infant was fed 30 min prior to MRI, fitted with silicone earplugs to mitigate scanner noise (Instaputty, E.A.R. Inc, Boulder, CO), and swaddled in a blanket and a vacuum immobilization device (MedVac, CFI Medical Solutions, Fenton, MI) to promote natural sleep. We acquired MRI data as follows: diffusion MRI: echo time 88 ms, repetition time 6972 ms, flip angle 90°, field of view 160 × 160 mm^2, 80 × 79 matrix, 2-mm contiguous slices, and scan time 5:58 min. 36 directions of diffusion gradients were applied with a b value of 800 s/mm^2 (4 b0 images were acquired with posterior-anterior phase encoding, and 1 b0 image was acquired with anterior-posterior phase encoding); axial T2-weighted image: echo time 166 ms, repetition time 18567 ms, flip angle 90°, voxel dimensions 1.0 × 1.0 × 1.0 mm^3, and scan time 3:43 min; Three-dimensional magnetization-prepared rapid gradient echo: echo time 3.4 ms, repetition time 7.3 ms, flip angle 11°, voxel dimensions 1.0 × 1.0 × 1.0 mm^3, and scan time 2:47 min; sagittal SWI: echo time 7.2 ms, repetition time 29 ms, flip angle 17°, voxel dimensions 0.57 × 0.57 × 1.0 mm^3, and scan time 3:27 min.

2.3. DWMA quantification

We quantified whole-brain DWMA on T2 images using our previously-described semi-automated software (He et al., 2013). Briefly, after preprocessing the T2 images with bias field correction and intensity normalization and performing tissue segmentation via a unified algorithm (Ashburner and Friston, 2005) with the guide of a neonatal atlas (Shi et al., 2011), our program designated white matter voxels as DWMA if their intensity was greater than 1.8 standard deviations above the mean intensity for all grey and white matter voxels, a cutoff determined by our previous research (Parikh et al., 2020) (Fig. 1). For each subject, we normalized whole-brain DWMA volume by the infant's total white matter volume to correct for the effect of brain size. The investigator who performed DWMA quantification was blinded to the results of the graph theory analysis, and vice versa.

2.4. Brain abnormality scoring

We used the standardized scoring system developed by Kidokoro et al. (2013); Harpster (2021) to derive a brain abnormality score for each study subject. The overall score is the sum of four individual scores quantifying the extent of abnormalities in 1) the cortical grey matter, 2) the cerebral white matter, 3) the deep grey matter, and 4) the cerebellum. A single pediatric neuroradiologist who was masked to the clinical history of the study subjects performed all qualitative and quantitative MR image assessments.

2.5. Diffusion MRI processing

We used standard FSL (http://fsl.fmrib.ox.ac.uk/fsl/fslwiki/, version 5.0.11) routines to preprocess the diffusion data, correcting for susceptibility-induced distortions (using the reverse phase-encoded b0 image), movement artifact, and eddy current-induced distortions. Diffusion Toolkit software allowed us to fit a tensor model in each brain voxel and generate maps of fractional anisotropy (FA), mean diffusivity (MD), radial diffusivity (RD), and axial diffusivity (AD) in diffusion space. From the FA maps, we performed whole-brain, deterministic fiber tracking with an angulation threshold of 35°. We linearly aligned each subject's T2-weighted image to their diffusion b0 image, to produce an image with more clearly-delineated anatomical boundaries than the original b0. We then aligned the 90-region automated anatomical labeling (AAL) infant template (Shi et al., 2011; Tzourio-Mazoyer et al., 2002) to this new image, to create parcellated brain maps in diffusion space. We visually inspected each resulting image to ensure that the template had aligned properly and that all regional boundaries were clearly and correctly delineated. For several subjects with initial suboptimal template alignment, we performed additional alignment of the image via the anterior and posterior commissures before reattempting alignment with the template.

2.6. Diffusion tensor metrics

The diffusion tensor (DT) model uses the diffusion signal in each brain voxel to estimate the underlying tissue microstructure. FA, one of the most commonly-derived DT metrics, measures the degree of directionality of the white matter fibers and can be considered a surrogate marker of overall white matter integrity. AD measures diffusion along an axon's main (longitudinal) axis, and RD quantifies the average diffusion in the other two orthogonal directions. MD, also known as apparent diffusion coefficient, captures the amount of diffusion in all three directions. In normal brain development, FA of the white matter tracts increases and MD, RD, and AD tend to decrease with age (Mukherjee et al., 2001). However, in preterm infants with DEHSI, FA is reduced and MD, RD, and AD are elevated in regions of DEHSI as compared to normal surrounding white matter, although AD is less straightforward than the other metrics. At least one study found that AD can both increase and decrease, depending on the brain region, in preterm infants with DWMA (Cheong et al., 2009). AD in particular is not sensitive to myelination, unlike the other three metrics of the DT model. (Feldman et al., 2010)

2.7. Brain structural connectome construction

We used the MRtrix3 software (http://www.mrtrix.org, version 0.3.0) to create undirected connectivity matrices weighted by the four major metrics from the diffusion tensor model (FA, MD, RD, or AD). For each metric, we extracted a value at each discrete point along every white matter streamline. We generated 90x90 conectivity matrices, the edge weights of which were the mean values for all streamlines connecting each regional pair. An edge could only exist where regions were connected by one or more streamline. For the RD, MD, and AD weighted networks, we used the inverse mean values, so that the edge weights roughly corresponded to white matter integrity, based on the expected trajectory in typical development. To avoid spurious associations due to noise in the diffusion image and because many regional pairs are not biologically plausible, we reassigned matrix elements with mean FA $<$ 0.05 to zero. To verify that this absolute threshold did not alter the overall picture of the preterm connectome, we examined the global efficiency values for each connectome calculated over a range of possible FA thresholds (0 to 0.2 in increments of 0.01) and verified that the values were stable (Supplementary Fig. 5). For our secondary analysis, we set elements with mean MD/RD/AD $< 5 \times 10^{-4}$ mm^2/sec to zero. We also set upper bounds of 0.0025 for MD and RD and 0.003 for AD, based on plausible values for the very preterm brain (Teli et al., 2018).

2.8. Graph theory metrics

We used the open-source, MATLAB-compatible Brain Connectivity Toolbox (www.brain-connectivity-toolbox.net) to calculate our graph theory metrics of interest. We computed global efficiency for each whole connectome and local efficiency and clustering coefficient for each region/node. Global efficiency of a network is defined as the average inverse shortest path length for that network (Achard and Bullmore, 2007), with path in this context describing the number of steps between regions rather than physical distance. Higher global efficiency represents fewer overall steps between nodes in a network, and as our networks are weighted by fractional anisotropy, higher FA values also

Table 1
Baseline characteristics of the final very preterm cohort and the excluded infants.

Characteristics	Final Cohort (n = 324)	Excluded (n = 19)	p
Antenatal steroids (completed course), n (%)	299 (92.3)	18 (94.7)	1.00
Gestational age, weeks, mean (SD)	29.3 (2.5)	28.4 (2.1)	0.09
Birth weight, grams, mean (SD)	1308.6 (459.4)	1174.1 (311.5)	0.10
Male, n (%)	162 (50.0)	5 (26.3)	0.06
Severe retinopathy of prematurity*, n (%)	18 (5.6)	1 (5.3)	1.00
Bronchopulmonary dysplasia, n (%)	115 (35.5)	11 (57.9)	0.08
Late onset sepsis, n (%)	30 (9.3)	3 (15.8)	0.41
Postnatal steroids (dexamethasone), n (%)	32 (9.9)	3 (15.8)	0.43
Maternal education (college degree or higher), n (%)	154 (47.5)	9 (47.4)	1.00
Private insurance, n (%)**	155 (48.3)	5 (26.3)	0.10
Household income above $60,000, n (%)	159 (49.1)	9 (47.4)	1.00
Moderate to severe injury on structural MRI, n (%)	30 (9.3)	9 (47.4)	*<0.001*

* 1 included subject did not have retinopathy of prematurity data.
** 3 included subjects did not have insurance data.

equate to higher global efficiency. Local efficiency is equivalent to global efficiency calculated on the neighborhood of a single node. The clustering coefficient (Latora and Marchiori, 2001) of a node is the fraction of the node's neighbors that are neighbors of each other, and as such it can be thought of as a measure of fault tolerance in the network.

2.9. Metric normalization

Because regional graph theory metrics can be influenced by both number of nodes (N) and the average degree (k) of a network (van Wijk et al., 2010) and because normalization has been shown to produce more robust features (Paldino et al., 2019), we normalized our regional metrics (E_{loc} and CC) two ways. 1) As the number of nodes was already constant across subjects (N = 90), we retained an equal number of strong connections across all networks. Given that the smallest number of unique connections in any network (after thresholding) was 569, we retained the strongest 550 unique connections for all networks before calculating our metrics of interest. This approach results in an equal average degree distribution for all networks (van Wijk et al., 2010). To verify that our results were robust across levels of network sparcity, we also report results when retaining the top 500 and top 450 strongest connections in the supplement. 2) Normalization via random graphs. As an alternate normalization approach, for each connectome, we created 100 random graphs with preserved degree distribution by randomly rewiring each edge 1000 times using Maslov and Sneppen's algorithm in Brain Connectivity Toolbox (Maslov and Sneppen, 2002). For this approach, we divided the nodal metrics calculated from each subject's connectome by the mean taken over all random networks for that subject.

2.10. Statistical analysis

Our primary analysis concerned the relationship between graph theory metrics derived from the FA-weighted connectivity matrices and DWMA extent. In Stata version 16.0 (StataCorp, College Station, TX), we performed partial correlation analysis between normalized DWMA volume and E_{glob}, E_{loc}, and CC, with the effects of PMA at MRI, gestational age, sex, structural brain abnormality (using the global brain abnormality score) (Kidokoro et al., 2013), birth hospital, and bronchopulmonary dysplasia (defined as supplemental oxygen use at 36 weeks PMA) removed. We applied Benjamini-Hochberg false discovery rate (FDR) correction to account for all 181 graph theory metrics examined (global efficiency, local efficiency for 90 regions, and clustering coefficient for 90 regions), with an accepted FDR of 5%. For our

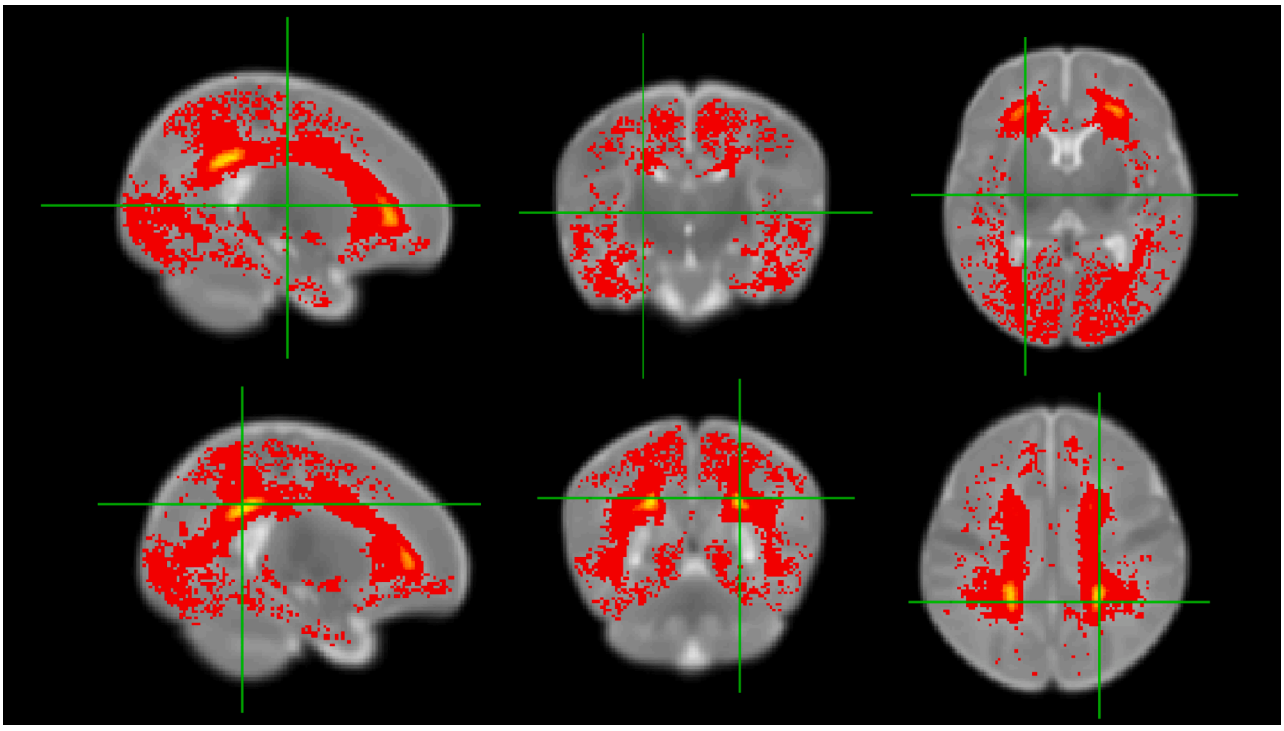

Fig. 2. Heatmap of DWMA concentration in the very preterm brain. 311 DWMA segmentations created by our algorithm were aligned to the AAL infantneo template using linear and nonlinear warping, to produce a heatmap of its location in our cohort. Two different views of the same map (top and bottom row) are shown from three perspectives. Yellow means that DWMA existed in a particular voxel for more subjects. (For interpretation of the references to colour in this figure legend, the reader is referred to the web version of this article.)

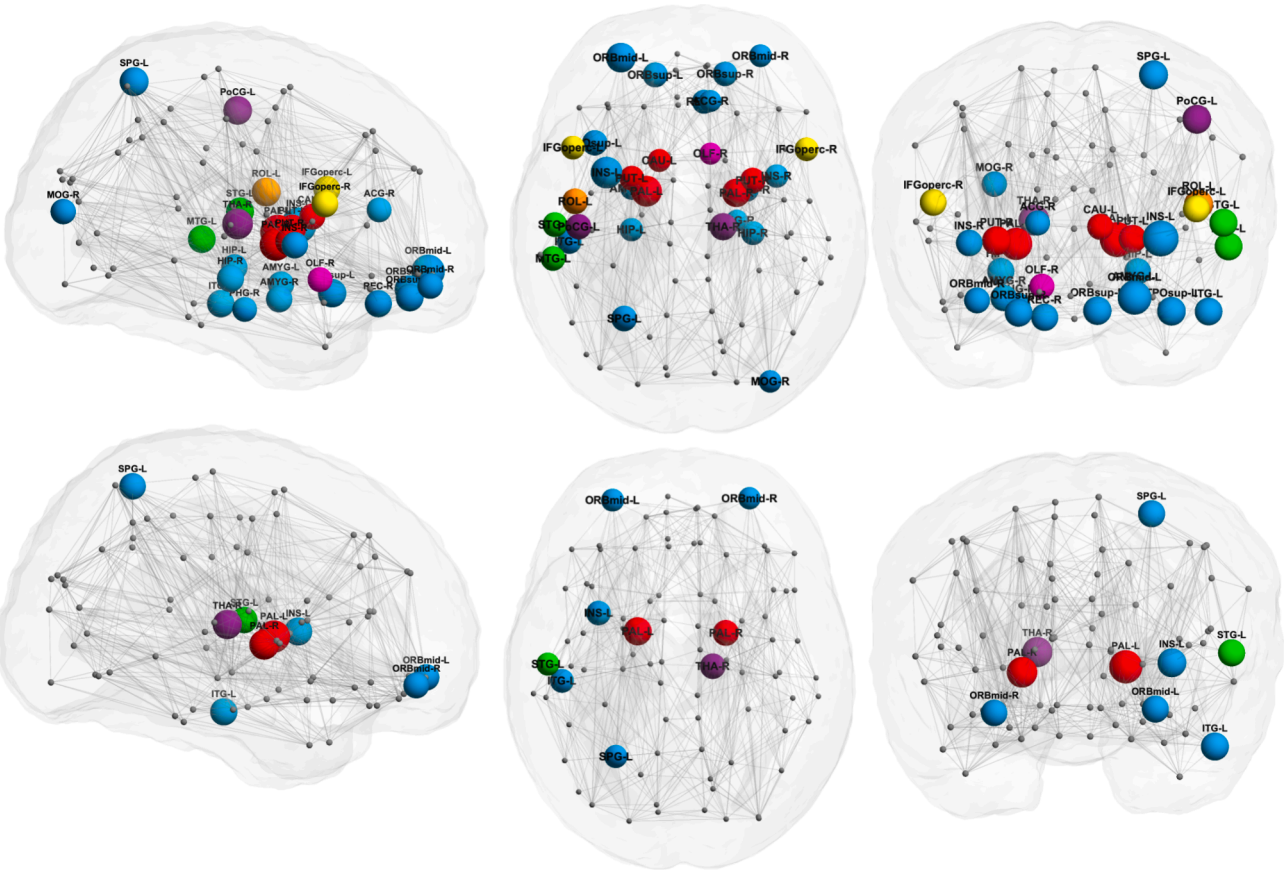

Fig. 3. DWMA vs regional LE and CC for FA-weighted structural networks. Nodes in which DWMA volume was negatively correlated with local efficiency (top) or clustering coefficient (bottom) in the very preterm brain, after covariate correction and FDR. There were no significant positive correlations. The networks are shown from sagittal (left), axial (middle), and coronal (right) perspectives. Colors represent network membership: blue = cognitive, yellow = language, red = motor, green = cognitive/language, purple = cognitive/motor, orange = language/motor, and pink = other. The size of each sphere represents the total variance explained in the covariate-corrected model of normalized DWMA volume.

secondary analysis, we repeated the above analysis for the MD, RD, and AD-weighted connectivity matrices, to help delineate the contribution of myelination vs axonal injury in DWMA pathology. We also repeated all of the aforementioned analyses after first applying our alternate normalization approach (normalization via random networks). Our brain networks were visualized using BrainNet Viewer (http://www.nitrc.org/projects/bnv/).

Additionally, we performed two minor analyses. First, to confirm the validity of our graph theory metrics, we examined the relationship of FA-weighted global efficiency, local efficiency, and clustering coefficient with overall brain abnormality score (and all four subdomains scores), with an expectation that all three graph metrics would be reduced with increasing abnormality. Second, to identify possible exclusion bias, we compared the baseline characteristics of our final cohort to the excluded infants. We used a Fischer's exact test for binary variables and either a Student's *t*-test or a Mann-Whitney *U* test for continuous variables, after assessing normality. All applicable significance tests were two-tailed, and a p-value of < 0.05 indicated significance.

3. Results

Out of an initial cohort of 343 very preterm infants with identically-acquired diffusion MRI scans, eight were excluded due to suboptimal alignment with the AAL template (Shi et al., 2011; Tzourio-Mazoyer et al., 2002), resulting from artifacts on diffusion MRI (n = 7) or deformational scaphocephaly (n = 1). An additional 11 subjects were excluded due to ventriculomegaly; in extreme cases very little brain tissue was spared for DWMA detection. Our final cohort comprised 324 infants with high-quality diffusion data and objectively-quantified DWMA. The mean (SD) postmenstrual age at MRI scan was 42.8 (1.3) weeks. Compared to our final cohort, excluded infants were more likely to have moderate or severe brain injury, which was expected due to the nature of the exclusions. All other baseline characteristics were comparable between the two groups. Table 1 summarizes the clinical characteristics of both cohorts as well as their statistical differences. Fig. 2 shows a heatmap of where DWMA tended to concentrate in the preterm brain.

As expected, mean graph theory measures derived from the FA-weighted connectivity matrices were significantly influenced by brain abnormality. Our final cohort had a median brain abnormality score of 2 and an interquartile range of 5. For our final cohort of 324, 216 subjects (66.7%) had no brain abnormality (scores of 0–3), 72 (22.2%) had mild abnormality (scores of 4–7), 19 (5.9%) had moderate abnormality (scores 8–11), and 17 (5.3%) had severe abnormality (scores $\geq$12). Brain abnormality score was negatively correlated with E_{glob} (r = -0.27, p = 8.60E-07), with E_{loc} in 24 nodes, and with CC in 18 nodes (Supplementary Fig. 1, Supplementary Table 1).

As hypothesized, E_{glob} of the FA-weighted brain networks was negatively correlated with DWMA volume (p = 2.27 E-04). Regarding the two normalization schemes, the regions identified as significantly related to DWMA extent overlapped substantially for all network weightings. We therefore present the results normalized by retaining an equal number of strongest connections (550) in the main text. The results for normalization via random networks can be found in the supplement (Supplementary Table 2, Supplementary Figs. 2–4). Regionally,

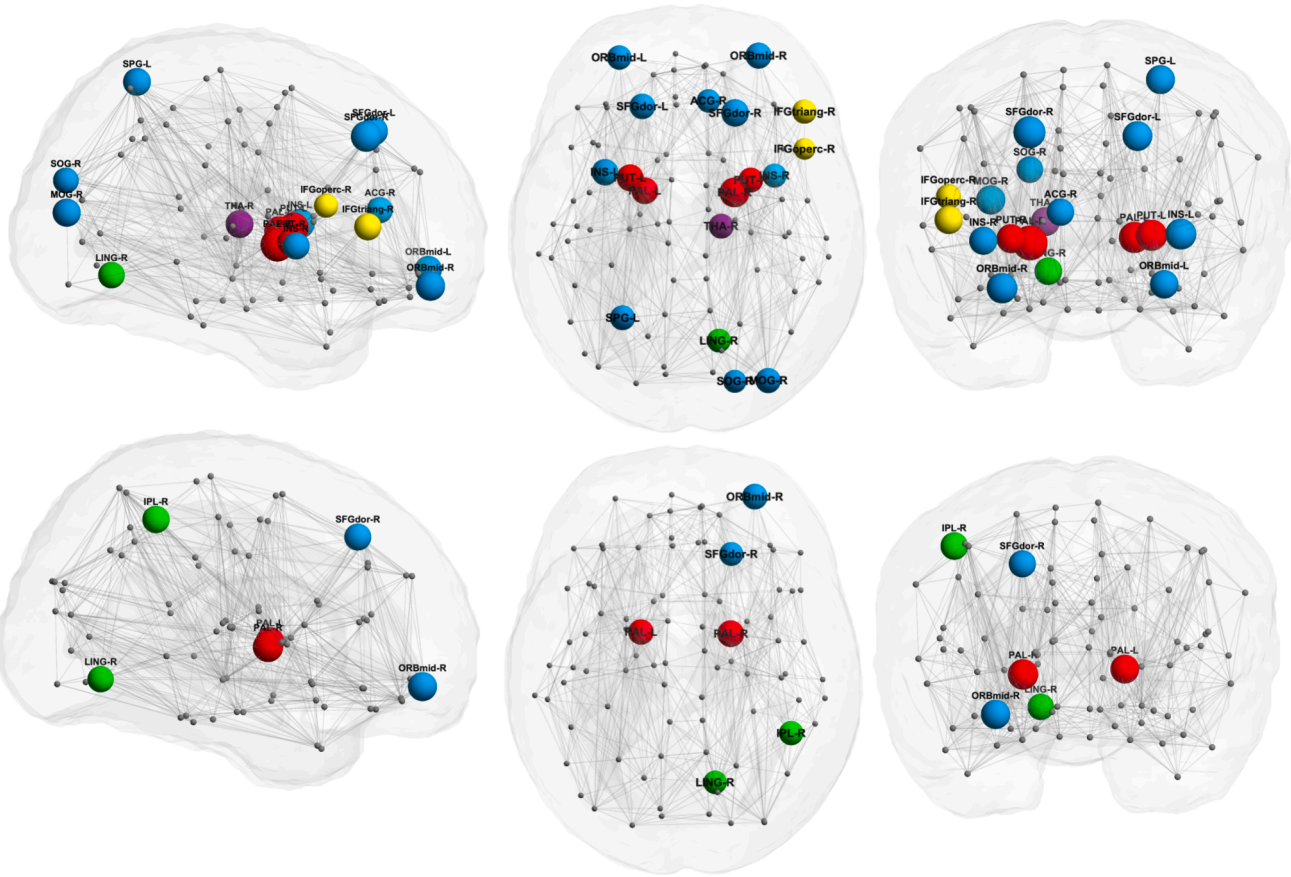

Fig. 4. DWMA vs regional LE and CC for inverse MD-weighted structural networks. Nodes in which DWMA volume was negatively correlated with local efficiency (top) or clustering coefficient (bottom) in the very preterm brain, after covariate correction and FDR. There were no significant positive correlations. The networks are shown from sagittal (left), axial (middle), and coronal (right) perspectives. Colors represent network membership: blue = cognitive, yellow = language, red = motor, green = cognitive/language, purple = cognitive/motor, orange = language/motor, and pink = other. The size of each sphere represents the total variance explained in the covariate-corrected model of normalized DWMA volume. (For interpretation of the references to colour in this figure legend, the reader is referred to the web version of this article.)

local efficiency was negatively correlated with DWMA in 30 nodes and CC was negatively correlated with DWMA in 9 nodes (Fig. 3, Table 2). There were no significant positive associations between DWMA volume and any graph theory metric tested. Similar results were seen across various levels of network sparcity (550, 500, or 450 strongest connections), although fewer nodal metrics remained significant as sparcity increased (Supplementary Table 3). Regional metrics with the strongest associations, for instance local efficiency of the left middle orbitofrontal cortex, right thalamus, and bilateral hippocampus and pallidum, remained strongly negatively associated with DWMA extent at all levels of sparcity tested.

The results of our secondary analysis show complementary but less widespread relationships between DWMA volume and graph theory metrics derived from the MD- and RD-weighted networks. For the MD-weighted networks, DWMA extent was negatively correlated with E_{glob} ($p = 0.02$), E_{loc} in 17 nodes, and CC in 6 nodes (Fig. 4, Table 2). For RD, DWMA was negatively correlated with E_{glob} ($p = 6.02E{-}04$), with E_{loc} in 26 nodes, and with CC in 16 nodes (Fig. 5, Table 2). For the AD-weighted networks, E_{glob} was not significantly related to DWMA extent and E_{loc} was only significantly correlated with DWMA in the triangular right inferior frontal gyrus ($p = 4.89E{-}05$, not shown). Of the 42 nodes in which E_{loc} or CC were significantly correlated with DWMA, nearly all could be ascribed to a cognitive, language, or motor function (Table 2).

4. Discussion

We have illustrated that in the very preterm brain at term-equivalent age, increasing volume of objectively-quantified DWMA is indicative of widespread reduced network efficiency as indexed by graph theoretical metrics. For FA-weighted structural connectomes, increased DWMA volume correlates with decreased global efficiency, local efficiency, and clustering coefficient throughout a widely-distributed brain network that subserves cognitive, language, and motor performance. This finding supports the idea that DWMA is a pathological signal related to decreased white matter structural integrity. Less-widespread yet complementary results were found for MD and RD-weighted networks, however there was only one significant region for the AD-weighted networks, which may offer insight into the pathophysiology of DWMA. The lack of an association with the AD networks suggests that abberent myelination rather than axonal injury is primarily at play in the pathophysiology of DWMA.

Alterations in diffusion metrics in the presence of DEHSI have been previously reported and are consistent with our findings. In a cohort of extremely preterm infants (GA < 27 weeks), Skiold and colleagues found that infants with qualitatively-diagnosed DEHSI had lower FA and higher apparent diffusion coefficient in the centrum semiovale and along the corpus collosum than infants without DEHSI (Skiöld, 2010). Counsell et al. reported that compared to infants with normal white matter, very preterm infants with qualitatively-defined DEHSI had elevated radial diffusivity in the posterior limb of the internal capsule and the corpus collosum and elevated axial and radial diffusivity in the frontal, occipital, and periventricular white matter and centrum semiovale (Counsell, 2006). Leitner et al. reported similar findings: elevated axial and radial diffusivities in the optic radiations, centrum semiovale,

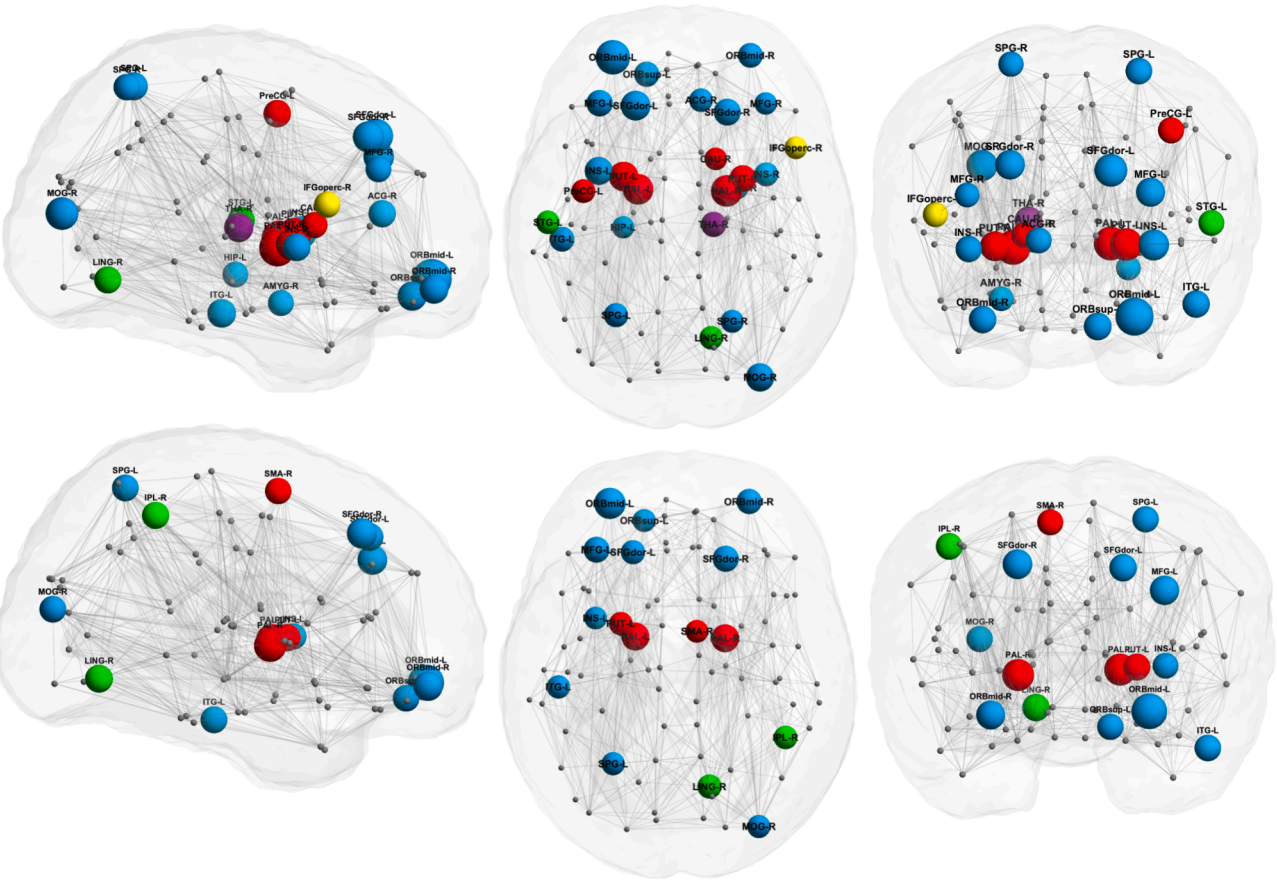

Fig. 5. DWMA vs regional LE and CC for inverse RD-weighted structural networks. Nodes in which DWMA volume was negatively correlated with local efficiency (top) or clustering coefficient (bottom) in the very preterm brain, after covariate correction and FDR. There were no significant positive correlations. The networks are shown from sagittal (left), axial (middle), and coronal (right) perspectives. Colors represent network membership: blue = cognitive, yellow = language, red = motor, green = cognitive/language, purple = cognitive/motor, orange = language/motor, and pink = other. The size of each sphere represents the total variance explained in the covariate-corrected model of normalized DWMA volume. (For interpretation of the references to colour in this figure legend, the reader is referred to the web version of this article.)

and posterior limb of the internal capsule in infants with DEHSI but without overt brain injury. (Leitner, 2014) All these findings suggest that in the presence of DWMA there is either 1) reduced myelination of white matter tracts or 2) an underlying axonal abnormality involving decreased white matter integrity or disorganized white matter microstructure.

Results from our postmortem histopathology case series (Parikh et al., 2016) indicated that both axonal loss and reduced myelination are in fact involved in DWMA pathology. Both of these microstructural abnormalities could manifest as decreased FA and increases in the other three diffusion metrics. However, given that metrics of efficiency from our FA/MD/RD networks were significantly associated with DWMA extent but AD-weighted efficiency metrics were not (with the exception of local efficiency in one node), we cautiously posit that DWMA pathology is driven more by myelination abnormalities than by severe axonal injury. This agrees with the notion that diffuse white matter disturbances in encephalopathy of prematurity are specifically characterized by injury to oligodencdrocytes (Volpe, 2011; Back, 2017). However, we cannot rule out that AD is a poorer DTI metric from which to infer the presence of pathology such as DWMA, due to the aforementioned conflict over its trajectory in typical development and following preterm birth (Cheong et al., 2009; Teli et al., 2018) and also conflicting accounts of how it is altered by axonal injury (Winklewski et al., 2018).

For the FA-weighted connectomes, local efficiency and clustering coefficient decreased with increasing DWMA volume throughout much of the very preterm brain, especially in regions related to cognition, language, and motor ability (Table 2), reinforcing the premise that DWMA extent is tied to the specific deficits often seen in preterm children (Parikh et al., 2020a, 2020b). FA-weighted E_{loc} and CC were consistently and strongly reduced with increasing DWMA volume in brain regions critical to cognitive function, especially in the bilateral insula, the left superior parietal gyrus, the left inferior temporal gyrus, and the bilateral middle orbitofrontal cortex, which is critical for decision making (Wallis, 2007). E_{loc} and CC were also negatively correlated with DWMA in nodes crucial to language production and comprehension, especially the bilateral inferior frontal gyrus (the left side of which contains Broca's area) and the left superior temporal gyrus, containing Wernicke's area. Furthermore, FA-weighted graph theory metrics were consistently down-regulated with increasing DWMA extent in several nodes of the brain's motor network, particularly the right thalamus and in the bilateral pallidum and putamen. The MD and RD networks lend support to this interpretation; all regional efficiency metrics that decreased significantly with DWMA can be ascribed to motor, language, and cognitive functions, and there was a high degree of regional overlap across all networks. See Table 2 for a complete list of the significant regions and a cursory listing of their membership within functional networks.

Graph theory applied to the preterm connectome has begun to delineate network changes associated with prematurity and tease apart the contributions of other factors like preterm illnesses. Bouyssi-Kobar et al. used resting state functional connectivity to compare the brains of preterm and full-term infants at term-equivalent age (Bouyssi-Kobar et al., 2019). They recorded decreased global efficiency, local efficiency,

Table 2
Nodes in which DWMA volume was significantly associated with local efficiency or clustering coefficient for FA, MD, and RD-weighted connectomes, after covariate correction and FDR. Significant p-values for local efficiency are in the top row of each cell, and significant p-values for clustering coefficient are in the bottom row.

Node	FA	MD	RD	Network
Precentral gyrus left PreCG-L			1.89E-03	Motor
Superior frontal gyrus (dorsal) left SFGdor-L		6.21E-04	4.92E-06 3.15E-03	Cognition
Superior frontal gyrus (dorsal) right SFGdor-R		8.71E-05 4.68E-03	1.52E-04 5.36E-04	Cognition
Orbitofrontal cortex (superior) left ORBsup-L	3.56E-04		5.00E-04 9.58E-03	Cognition
Orbitofrontal cortex (superior) right ORBsup-R	1.10E-03			Cognition
Middle frontal gyrus left MFG-L			2.74E-04 6.08E-04	Cognition
Middle frontal gyrus right MFG-R			1.09E-02	Cognition
Orbitofrontal cortex (middle) left ORBmid-L	8.74E-06 9.00E-03	2.33E-03	4.56E-08 2.15E-06	Cognition
Orbitofrontal cortex (middle) right ORBmid-R	7.41E-03 8.17E-03	1.61E-04 3.61E-04	4.81E-04 4.92E-04	Cognition
Inferior frontal gyrus (opercular) left IFGoperc-L	3.19E-03			Language
Inferior frontal gyrus (opercular) right IFGoperc-R	4.25E-03		8.75E-03	Language
Inferior frontal gyrus (triangular) right IFGtriang-R*		1.52E-03		Language
Rolandic operculum left ROL-L	5.12E-04			Language Motor
Supplementary motor area right SMA-R			1.01E-02	Motor
Olfactory right OLF-R	9.60E-03			
Rectus gyrus right REC-R	2.15E-03			Cognition
Insula left INS-L	1.04E-07 5.38E-04	1.22E-04	1.16E-05 9.59E-03	Cognition
Insula right INS-R	1.85E-03	1.93E-03	1.26E-03	Cognition
Anterior cingulate gyrus right ACG-R	1.09E-02	2.33E-03	2.22E-03	Cognition
Hippocampus left HIP-L	1.49E-03		5.73E-03	Cognition
Hippocampus right HIP-R	4.04E-04			Cognition
Parahippocampal gyrus right PHG-R	1.02E-02			Cognition
Amygdala left AMYG-L	4.07E-03			Cognition
Amygdala right AMYG-R	3.28E-03		8.28E-03	Cognition
Lingual gyrus right LING-R		2.16E-03	1.70E-03	CognitionLanguage
		4.58E-03	1.68E-03	
Superior occipital gyrus right SOG-R		4.96E-03		Cognition
Middle occipital gyrus right MOG-R	9.75E-03	6.19E-04	7.81E-06 7.57E-03	Cognition
Postcentral gyrus left PoCG-L	5.28E-04			CognitionMotor
Superior parietal gyrus left SPG-L	2.89E-04 5.26E-03	8.59E-04	1.07E-03 7.07E-03	Cognition
Superior parietal gyrus right SPG-R			5.07E-03	Cognition
Inferior parietal lobule right IPL-R		3.11E-03	5.71E-03	CognitionLanguage
Caudate left CAU-L	8.48E-04			Motor
Caudate right CAU-R			8.18E-03	Motor
Putamen left PUT-L	5.35E-04	9.04E-05	2.23E-06 4.70E-03	Motor
Putamen right PUT-R	1.41E-04	3.97E-04	1.71E-05	Motor
Pallidum left PAL-L	4.82E-07 1.46E-05	1.19E-04 7.64E-04	9.63E-07 4.19E-05	Motor
Pallidum right PAL-R	7.43E-06 1.73E-04	3.86E-06 1.61E-04	3.28E-07 3.82E-05	Motor
Thalamus right THA-R	1.98E-05 1.20E-04	7.54E-04	3.61E-04	CognitionMotor
Superior temporal gyrus left STG-L	1.04E-03 5.05E-03		2.29E-03	CognitionLanguage
Temporal pole (superior) left TPOsup-L	4.70E-04			Cognition
Middle temporal gyrus left MTG-L	1.60E-03			CognitionLanguage
Inferior temporal gyrus left ITG-L	1.41E-03 2.20E-03		4.13E-04 4.51E-03	Cognition

*Means that LE was also significant for AD connectomes.

and clustering coefficient in the preterm brain and determined an association with chronic respiratory illness. We found that the same graph theory metrics are decreased in proportion to DWMA volume (even when correcting for a common neonatal respiratory illness, bronchopulmonary dysplasia), suggesting that DWMA is a robust biomarker of network disorganization in the preterm brain at term with independent significance. Network alterations associated with prematurity persist into early life, as Young et al. reported decreased E_{glob}, E_{loc}, and CC in very preterm children compared to full-term children at four years of age (Young, 2018). Thompson et al. showed decreased E_{glob} but increased E_{loc} in specific brain regions in preterm children at seven years of age (Thompson et al., 2016), a discrepancy which may suggest that preterm children employ compensatory strategies to improve the efficiency of specific brain regions during early life.

Our study has a number of strengths. We recruited a regional, population-based cohort of very preterm infants, thus increasing the generalizability of our findings. This is the largest cohort ever assembled

to study DWMA, which may explain why we identified such a strong association between DWMA and global efficiency of the preterm brain for the FA, MD, and RD-weighted networks, which remained highly significant after correction for several confounding variables. Unlike most prior studies, we used an semi-automated, objective method to quantify DWMA. To our knowledge, only one other group has developed an algorithm to accurately segment DWMA (Xu et al., 2018), however it has not been validated with clinical outcomes like our algorithm (Parikh et al., 2020; Parikh, 2020). Furthermore, by using graph theory rather than diffusion metrics alone, we were able to identify high-level network changes associated with DWMA extent. Finally, we examined structural connectomes weighted by several measures from the diffusion tensor model to disambiguate the relationship between DWMA and brain network alterations. However, our study also had some limitations. Excluded subjects were more likely to have moderate to severe brain injury, which may have introduced some sample bias. Nevertheless, our findings remained significant after controlling for structural abnormalities on MRI using global brain abnormality score.

5. Conclusions

Overall, increasing volume of objectively-quantified DWMA is correlated with reduced information processing efficiency throughout the very preterm brain, as indexed by graph theoretical metrics, especially global efficiency and local efficiency. Our work suggests that the most common MRI finding in very preterm infants at term is associated with decreased brain network efficiency, due in large part to abnormal myelination compromising information transfer throughout the network. Furthermore, the consistent results across various network weightings and normalization schemes help identify and affirm which brain regions are preferentially impacted by DWMA. More work is warranted to determine the exact interplay between DWMA, brain network efficiency, and neurodevelopmental outcomes later in life. We have begun to undertake these follow-up studies in our center.

Data availability

Code used in this analysis and derived data that support the conclusions of this study are available upon direct request to the corresponding author.

CRediT authorship contribution statement

Julia E. Kline: Data curation, Formal analysis, Writing - original draft, Investigation, Methodology, Resources, Software, Validation, Visualization. **Venkata Sita Priyanka Illapani:** Data curation, Formal analysis, Resources, Software, Validation. **Hailong Li:** Data curation, Formal analysis, Investigation, Methodology, Resources, Software, Validation. **Lili He:** Data curation, Resources, Software, Methodology. **Weihong Yuan:** Methodology, Resources, Validation. **Nehal A. Parikh:** Conceptualization, Data curation, Formal analysis, Funding acquisition, Investigation, Methodology, Project administration, Resources, Supervision.

Acknowledgements

This research was supported by grants R01-NS094200-05 and R01-NS096037-03 from the National Institute of Neurological Disorders and Stroke (NINDS), R21-HD094085 from the Eunice Shriver Kennedy National Institute of Child Health and Human Development (NICHD), and R01-EB029944 from the National Institute of Biomedical Imaging and Bioengineering. We sincerely thank the parents of infants that participated in our study and the Cincinnati Infant Neurodevelopment Early Prediction Study (CINEPS) Investigators

Principal Investigator

Nehal A. Parikh, DO, MS. Collaborators (in alphabetical order)

Mekibib Altaye, PhD, Anita Arnsperger, RRT, Traci Beiersdorfer, RN BSN, Kaley Bridgewater, RT(MR) CNMT, Tanya Cahill, MD, Kim Cecil, PhD, Kent Dietrich, RT, Christen Distler, BSN RNC-NIC, Juanita Dudley, RN BSN, Brianne Georg, BS, Cathy Grisby, RN BSN CCRC, Lacey Haas, RT(MR) CNMT, Karen Harpster, PhD, OT/RL, Lili He, PhD, Scott K. Holland, PhD, V.S. Priyanka Illapani, MS, Kristin Kirker, CRC, Julia E. Kline, PhD, Beth M. Kline-Fath, MD, Hailong Li, PhD, Matt Lanier, RT (MR) RT(R), Stephanie L. Merhar, MD MS, Greg Muthig, BS, Brenda B. Poindexter, MD MS, David Russell, JD, Kari Tepe, BSN RNC-NIC, Leanne Tamm, PhD, Julia Thompson, RN BSN, Jean A. Tkach, PhD, Hui Wang, PhD, Jinghua Wang, PhD, Brynne Williams, RT(MR) CNMT, Kelsey Wineland, RT(MR) CNMT, Sandra Wuertz, RN BSN CCRP, Donna Wuest, AS, Weihong Yuan, PhD.

Appendix A. Supplementary data

Supplementary data to this article can be found online at https://doi.org/10.1016/j.nicl.2021.102739.

References

Skiöld, B., et al., 2010. White matter changes in extremely preterm infants, a population-based diffusion tensor imaging study. Acta Paediatr. Int. J. Paediatr. 99, 842–849.

Jeon, T.Y., Kim, J.H., Yoo, S.-Y., Eo, H., Kwon, J.-Y., Lee, J., Lee, M., Chang, Y.S., Park, W.S., 2012. Neurodevelopmental outcomes in preterm infants: Comparison of infants with and without diffuse excessive high signal intensity on MR images at near-term-equivalent age. Radiology 263 (2), 518–526.

Kidokoro, H., Anderson, P.J., Doyle, L.W., Neil, J.J., Inder, T.E., 2011. High signal intensity on T2-weighted MR imaging at term-equivalent age in preterm infants does not predict 2-year neurodevelopmental outcomes. Am. J. Neuroradiol. 32, 2005–2010.

Broström, L., Bolk, J., Padilla, N., Skiöld, B., Eklöf, E., Mårtensson, G., Vollmer, B., Ådén, U., Parikh, N.A., 2016. Clinical Implications of diffuse excessive high signal intensity (DEHSI) on neonatal MRI in school age children born extremely preterm. PLoS One 11 (2), e0149578. https://doi.org/10.1371/journal.pone.014957810.1371/journal.pone.0149578.g00110.1371/journal.pone.0149578.g00210.1371/journal.pone.0149578.t00110.1371/journal.pone.0149578.t00210.1371/journal.pone.0149578.t00310.1371/journal.pone.0149578.s001.

Hart, A., et al., 2011. Neuro-developmental outcome at 18 months in premature infants with diffuse excessive high signal intensity on MR imaging of the brain. Pediatr. Radiol. 41, 1284–1292.

de Bruïne, F.T., van den Berg-Huysmans, A.A., Leijser, L.M., Rijken, M., Steggerda, S.J., van der Grond, J., van Wezel-Meijler, G., 2011. Clinical implications of MR imaging findings in the white matter in very preterm infants: A 2-year follow-up study. Radiology 261 (3), 899–906.

Skiöld, B., et al., 2012. Neonatal magnetic resonance imaging and outcome at age 30 months in extremely preterm infants. J. Pediatr. 160, 559–566.

Mürner-Lavanchy, I.M., Kidokoro, H., Thompson, D.K., Doyle, L.W., Cheong, J.L.Y., Hunt, R.W., Inder, T.E., Anderson, P.J., 2019. Thirteen-Year Outcomes in Very Preterm Children Associated with Diffuse Excessive High Signal Intensity on Neonatal Magnetic Resonance Imaging. J. Pediatr. 206, 66–71.e1.

Calloni, S.F., et al., 2015. Neurodevelopmental outcome at 36 months in very low birth weight premature infants with MR diffuse excessive high signal intensity (DEHSI) of cerebral white matter. Radiol. Medica 120, 1056–1063.

Leitner, Y., et al., 2014. Diffuse excessive high signal intensity in low-risk preterm infants at term-equivalent age does not predict outcome at 1 year: A prospective study. Neuroradiology 56, 669–678.

Boardman, J.P., Craven, C., Valappil, S., Counsell, S.J., Dyet, L.E., Rueckert, D., Aljabar, P., Rutherford, M.A., Chew, A.T.M., Allsop, J.M., 2010. A common neonatal image phenotype predicts adverse neurodevelopmental outcome in children born preterm. Neuroimage 52 (2), 409–414.

Krishnan, M.L., Dyet, L.E., Boardman, J.P., Kapellou, O., Allsop, J.M., Cowan, F., Edwards, A.D., Rutherford, M.A., Counsell, S.J., 2007. Relationship between white matter apparent diffusion coefficients in preterm infants at term-equivalent age and developmental outcome at 2 years. Pediatrics 120 (3), e604–e609.

Iwata, S., Nakamura, T., Hizume, E., Kihara, H., Takashima, S., Matsuishi, T., Iwata, O., 2012. Qualitative brain MRI at term and cognitive outcomes at 9 years after very preterm birth. Pediatrics 129 (5), e1138–e1147.

Iwata, S., et al., 2007. Abnormal white matter appearance on term FLAIR predicts neurodevelopmental outcome at 6 years old following preterm birth. Int. J. Dev. Neurosci. 25, 523–530.

Parikh, N.A., et al., 2013. Automatically quantified diffuse excessive high signal intensity on mri predicts cognitive development in preterm infants. Pediatr. Neurol. 49, 424–430.

Parikh, N.A., Harpster, K., He, L., Illapani, V.S.P., Khalid, F.C., Klebanoff, M.A., O'Shea, T.M., Altaye, M., 2020aa. Novel diffuse white matter abnormality biomarker at term-equivalent age enhances prediction of long-term motor development in very preterm children. Sci. Rep. 10 (1) https://doi.org/10.1038/s41598-020-72632-0.

Parikh, N.A., He, L., Priyanka Illapani, V.S., Altaye, M., Folger, A.T., Yeates, K.O., 2020bb. Objectively Diagnosed Diffuse White Matter Abnormality at Term Is an Independent Predictor of Cognitive and Language Outcomes in Infants Born Very Preterm. J. Pediatr. 220, 56–63. https://doi.org/10.1016/j.jpeds.2020.01.034.

Counsell, S.J., 2006. Axial and radial diffusivity in preterm infants who have diffuse white matter changes on magnetic resonance imaging at term-equivalent age. Pediatrics 117 (2), 376–386.
He, L., Parikh, N.A., 2015. Aberrant Executive and Frontoparietal Functional Connectivity in Very Preterm Infants with Diffuse White Matter Abnormalities. Pediatr. Neurol. 53, 330–337.
Parikh, N.A., Pierson, C.R., Rusin, J.A., 2016. Neuropathology Associated With Diffuse Excessive High Signal Intensity Abnormalities on Magnetic Resonance Imaging in Very Preterm Infants. Pediatr. Neurol. 65, 78–85.
Bullmore, E., Sporns, O., 2009. Complex brain networks: Graph theoretical analysis of structural and functional systems. Nat. Rev. Neurosci. 10, 186–198.
Rubinov, M., Sporns, O., 2010. Complex network measures of brain connectivity: Uses and interpretations. Neuroimage 52 (3), 1059–1069.
Sporns, O., Zwi, J.D., 2004. The small world of the cerebral cortex. Neuroinformatics 2 (2), 145–162.
Sporns, O., 2013. Structure and function of complex brain networks. Dialogues Clin. Neurosci. 15, 247–262.
Bassett, D.S., Khambhati, A.N., Grafton, S.T., 2017. Emerging Frontiers of Neuroengineering: A Network Science of Brain Connectivity. Annu. Rev. Biomed. Eng. 19, 327–352.
Ball, G., Aljabar, P., Zebari, S., Tusor, N., Arichi, T., Merchant, N., Robinson, E.C., Ogundipe, E., Rueckert, D., Edwards, A.D., Counsell, S.J., 2014. Rich-club organization of the newborn human brain. Proc. Natl. Acad. Sci. U. S. A. 111 (20), 7456–7461. https://doi.org/10.1073/pnas.1324118111.
Scheinost, D., Kwon, S.H., Shen, X., Lacadie, C., Schneider, K.C., Dai, F., Ment, L.R., Constable, R.T., 2016. Preterm birth alters neonatal, functional rich club organization. Brain Struct. Funct. 221 (6), 3211–3222. https://doi.org/10.1007/s00429-015-1096-6.
Bouyssi-Kobar, M., De Asis-Cruz, J., Murnick, J., Chang, T., Limperopoulos, C., 2019. Altered Functional Brain Network Integration, Segregation, and Modularity in Infants Born Very Preterm at Term-Equivalent Age. J. Pediatr. 213, 13–21.e1.
Young, J.M., et al., 2018. Altered white matter development in children born very preterm. Brain Struct. Funct. 223, 2129–2141.
Gozdas, E., et al., 2018. Altered functional network connectivity in preterm infants: antecedents of cognitive and motor impairments? Brain Struct. Funct. 223, 3665–3680.
Thompson, D.K., Chen, J., Beare, R., Adamson, C.L., Ellis, R., Ahmadzai, Z.M., Kelly, C.E., Lee, K.J., Zalesky, A., Yang, J.Y.M., Hunt, R.W., Cheong, J.L.Y., Inder, T.E., Doyle, L.W., Seal, M.L., Anderson, P.J., 2016. Structural connectivity relates to perinatal factors and functional impairment at 7 years in children born very preterm. Neuroimage 134, 328–337.
He, L., Parikh, N.A., Chen, K., 2013. Atlas-guided quantification of white matter signal abnormalities on term-equivalent age MRI in very preterm infants: Findings predict language and cognitive development at two years of age. PLoS One 8 (12), e85475. https://doi.org/10.1371/journal.pone.008547510.1371/journal.pone.0085475.g00110.1371/journal.pone.0085475.g00210.1371/journal.pone.0085475.g00310.1371/journal.pone.0085475.g00410.1371/journal.pone.0085475.g005.
Ashburner, J., Friston, K.J., 2005. Unified segmentation. Neuroimage 26 (3), 839–851.
Shi, F., Yap, P.-T., Wu, G., Jia, H., Gilmore, J.H., Lin, W., Shen, D., Okazawa, H., 2011. Infant brain atlases from neonates to 1- and 2-year-olds. PLoS One 6 (4), e18746. https://doi.org/10.1371/journal.pone.001874610.1371/journal.pone.0018746.g00110.1371/journal.pone.0018746.g00210.1371/journal.pone.0018746.g00310.1371/journal.pone.0018746.g00410.1371/journal.pone.0018746.g00510.1371/journal.pone.0018746.g00610.1371/journal.pone.0018746.g00710.1371/journal.pone.0018746.g00810.1371/journal.pone.0018746.g00910.1371/journal.pone.0018746.g01010.1371/journal.pone.0018746.t00110.1371/journal.pone.0018746.t002.
Parikh, N.A., He, L., Li, H., Priyanka Illapani, V.S., Klebanoff, M.A., 2020. Antecedents of Objectively-Diagnosed Diffuse White Matter Abnormality in Very Preterm Infants. Pediatr. Neurol. 106, 56–62.
Kidokoro, H., Neil, J.J., Inder, T.E., 2013. New MR imaging assessment tool to define brain abnormalities in very preterm infants at term. Am. J. Neuroradiol. 34, 2208–2214.
Harpster, K., et al., 2021. Associations Between Early Structural MRI, Hammersmith Infant Neurological Exam, and General Movements Assessment in Very Preterm Infants. J. Pediatr. https://doi.org/10.1016/j.jpeds.2020.12.056.
Tzourio-Mazoyer, N., Landeau, B., Papathanassiou, D., Crivello, F., Etard, O., Delcroix, N., Mazoyer, B., Joliot, M., 2002. Automated anatomical labeling of activations in SPM using a macroscopic anatomical parcellation of the MNI MRI single-subject brain. Neuroimage 15 (1), 273–289.
Mukherjee, P., Miller, J.H., Shimony, J.S., Conturo, T.E., Lee, B.C.P., Almli, C.R., McKinstry, R.C., 2001. Normal brain maturation during childhood: Developmental trends characterized with diffusion-tensor MR imaging. Radiology 221 (2), 349–358. https://doi.org/10.1148/radiol.2212001702.
Cheong, J.L.Y., Thompson, D.K., Wang, H.X., Hunt, R.W., Anderson, P.J., Inder, T.E., Doyle, L.W., 2009. Abnormal white matter signal on MR imaging is related to abnormal tissue microstructure. Am. J. Neuroradiol. 30 (3), 623–628. https://doi.org/10.3174/ajnr.A1399.
Feldman, H. M., Yeatman, J. D., Lee, E. S., Barde, L. H. F. Gaman-Bean, S., 2010. Diffusion tensor imaging: A review for pediatric researchers and clinicians. J. Dev. Behav. Pediatr. (2010). doi:10.1097/DBP.0b013e3181dcaa8b.
Teli, R., Hay, M., Hershey, A., Kumar, M., Yin, H., Parikh, N.A., 2018. Postnatal Microstructural Developmental Trajectory of Corpus Callosum Subregions and Relationship to Clinical Factors in Very Preterm Infants /692/308/3187 /692/617/375 /123 /119 article. Sci. Rep. 8 (1) https://doi.org/10.1038/s41598-018-25245-7.
Achard, S., Bullmore, E., 2007. Efficiency and cost of economical brain functional networks. PLoS Comput. Biol. 3, e17.
Latora, V., Marchiori, M., 2001. Efficient behavior of small-world networks. Phys. Rev. Lett. 87, 198701.
van Wijk, B.C.M., Stam, C.J., Daffertshofer, A., Sporns, O., 2010. Comparing brain networks of different size and connectivity density using graph theory. PLoS One 5 (10), e13701. https://doi.org/10.1371/journal.pone.001370110.1371/journal.pone.0013701.g00110.1371/journal.pone.0013701.g00210.1371/journal.pone.0013701.g00310.1371/journal.pone.0013701.g00410.1371/journal.pone.0013701.g00510.1371/journal.pone.0013701.g00610.1371/journal.pone.0013701.g00710.1371/journal.pone.0013701.t00110.1371/journal.pone.0013701.t00210.1371/journal.pone.0013701.s00110.1371/journal.pone.0013701.s00210.1371/journal.pone.0013701.s00310.1371/journal.pone.0013701.s00410.1371/journal.pone.0013701.s00510.1371/journal.pone.0013701.s006.
Paldino, M.J., Golriz, F., Zhang, W., Chu, Z.D., Sethi, T., 2019. Normalization enhances brain network features that predict individual intelligence in children with epilepsy. PLoS One 14 (3), e0212901. https://doi.org/10.1371/journal.pone.021290110.1371/journal.pone.0212901.g00110.1371/journal.pone.0212901.t00110.1371/journal.pone.0212901.t00210.1371/journal.pone.0212901.t00310.1371/journal.pone.0212901.t004.
Maslov, S., Sneppen, K., 2002. Specificity and stability in topology of protein networks. Science 80-,). https://doi.org/10.1126/science.1065103.
Volpe, J.J., 2011. Systemic inflammation, oligodendroglial maturation, and the encephalopathy of prematurity. Annals of Neurology 70 (4), 525–529. https://doi.org/10.1002/ana.v70.410.1002/ana.22533.
Back, S.A., 2017. White matter injury in the preterm infant: pathology and mechanisms. Acta Neuropathologica 134 (3), 331–349. https://doi.org/10.1007/s00401-017-1718-6.
Winklewski, P.J., Sabisz, A., Naumczyk, P., Jodzio, K., Szurowska, E., Szarmach, A., 2018. Understanding the physiopathology behind axial and radial diffusivity changes-what do we Know? Frontiers in Neurology 9. https://doi.org/10.3389/fneur.2018.00092.
Wallis, J.D., 2007. Orbitofrontal cortex and its contribution to decision-making. Annual Review of Neuroscience 30 (1), 31–56. https://doi.org/10.1146/annurev.neuro.30.051606.094334.
Xu, Y., Morel, B., Dahdouh, S., Puybareau, É., Virzì, A., Urien, H., Géraud, T., Adamsbaum, C., Bloch, I., 2018. The challenge of cerebral magnetic resonance imaging in neonates: A new method using mathematical morphology for the segmentation of structures including diffuse excessive high signal intensities. Med. Image Anal. 48, 75–94. https://doi.org/10.1016/j.media.2018.05.003.
Parikh, N.A., et al., 2020. Novel diffuse white matter abnormality biomarker at term-equivalent age enhances prediction of long-term motor development in very preterm children. Sci. Rep. 10, 1–9.